iScience

CellPress
OPEN ACCESS

Article

Long-term and potent IOP-lowering effect of IκBα-siRNA in a nonhuman primate model of chronic ocular hypertension

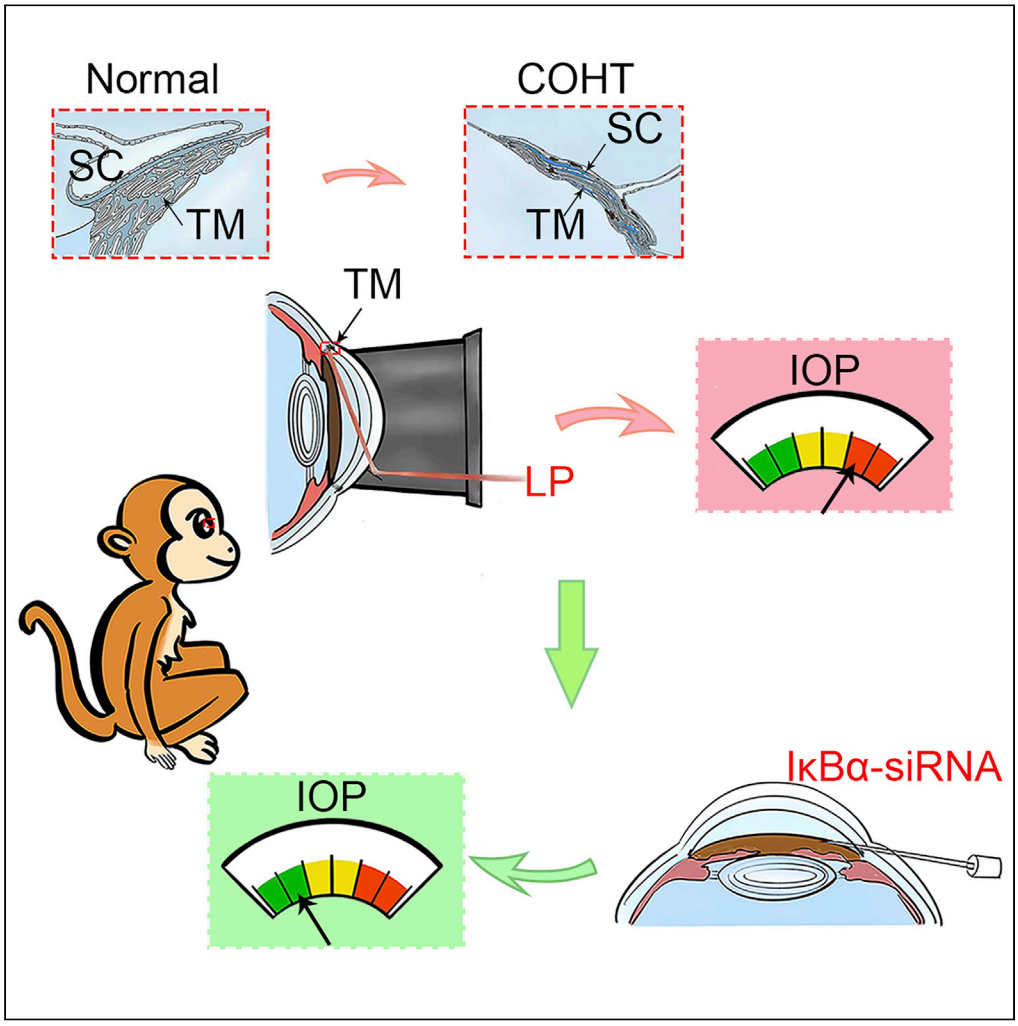

Difang Sun, Zongyi Zhan, Rui Zeng, ..., Zhenlan Yang, Yuanyuan Su, Yuqing Lan

lanyq@mail.sysu.edu.cn (Y.L.)
suyy36@mail.sysu.edu.cn (Y.S.)

Highlights

Knocking down IκBα could upregulate the expression of MMP2 and MMP9 in MCM and MTM

LP could induce COHT model in rhesus monkeys successfully

IκBα-siRNA has a long-term and potent IOP-lowering effect in LP-induced monkeys with COHT

Sun et al., iScience 25, 104149
April 15, 2022
https://doi.org/10.1016/j.isci.2022.104149

iScience

CellPress
OPEN ACCESS

Article

Long-term and potent IOP-lowering effect of IκBα-siRNA in a nonhuman primate model of chronic ocular hypertension

Difang Sun,[1,5] Zongyi Zhan,[1,5] Rui Zeng,[1] Xiaolin Liu,[2] Bin Wang,[3] Fan Yang,[1] Sa Huang,[2] Yunfeng Li,[2] Zhenlan Yang,[1] Yuanyuan Su,[4,*] and Yuqing Lan[1,6,*]

SUMMARY

Glaucoma is one of the most common causes of irreversible blindness. It is acknowledged that lowering intraocular pressure (IOP) is the effective treatment to slow glaucoma disease progression. The main obstacle of existing drugs is that the effect of reducing IOP does not last long. Degradation of IκB stimulates the transcription of NF-κB, which could upregulate the expression of matrix metalloproteinases (MMPs). Whether a IκB-targeted gene therapy works in glaucoma is unclear. Here, we established a chronic ocular hypertension (COHT) model in rhesus monkey by laser photocoagulation and verified that intracameral delivery of IκBα-siRNA showed long-lasting and potent effects of reducing IOP without obvious inflammation in monkeys with COHT. We also verified that IκBα-siRNA could increase the expressions of MMP2 and MMP9 by knocking down IκBα *in vitro* and *in vivo*. Our results in nonhuman primates indicated that IκBα-siRNA may become a promising therapeutic approach for the treatment of glaucoma.

INTRODUCTION

Glaucoma is a multifactorial progressive neurodegenerative disease characterized by irreversible loss of visual function, which affected almost 76.5 million people worldwide in 2020 and is estimated to reach 111.8 million by 2040 (Baudouin et al., 2021). Although there are many causes of glaucoma progression, intraocular pressure (IOP) remains the major risk factor, so as to reduce IOP is the main therapeutic mechanism for slowing disease progression in patients with glaucoma (Garway-Heath et al., 2015; Varma et al., 2011). However, existing drugs are limited due to several reasons, such as the inability of monotherapy to achieve the therapeutic target IOP, drug-related side effects, and the low compliance of patients to take multiple eye drops every day. Thus, in recent years, scientific and medical circles have paid more attention to the development of potent and long-acting new drugs to reduce IOP. However, until now, no FDA-approved drugs targeting the long-acting efficiency in reducing IOP of glaucoma have been developed.

Nonhuman primates, which are homologous with humans, constitute an indispensable laboratory model for various fields of biomedical research (Evans and Silvestri, 2013; Roelfsema and Treue, 2014; Tomalka et al., 2021; Wegener et al., 2021), and have become ideal glaucoma experimental animals because of their highly consistent anatomical structure and physiological characteristics with humans eyeballs (Pasquale et al., 2021; Rasmussen and Kaufman, 2005; Stewart et al., 2011). There are several kinds of chronic ocular hypertension (COHT) model in nonhuman primates, including topical dexamethasone treatment (steroid-induced glaucoma), intracameral injection of microbeads made of different materials, and laser photocoagulation (LP) of the trabecular meshwork (TM) (Fingert et al., 2001; Pelzel et al., 2006; Quigley and Hohman, 1983; Tu et al., 2019; Weber and Harman, 2005). Dexamethasone (Dex)-induced ocular hypertension is one of the most commonly used and developed murine ocular hypertension model (Kasetti et al., 2018; Zode et al., 2014), but the success rate of this model in nonhuman primates is only 45% with a short maintenance time (approximately 2 weeks) of high IOP after stopping medication (Fingert et al., 2001). Injection of microbeads with different materials in the anterior chamber could induce a model of chronic glaucoma, but invasive and repeated intracameral injections to maintain stable IOP are needed (Chen et al., 2011; Rodrigo et al., 2021; Samsel et al., 2011; Weber and Harman, 2005). Compared with Dex-induced and microbeads-induced COHT, LP-induced COHT is more advanced, due to the advantages of being noninvasive, having a mild inflammatory response, keeping the refractive stroma clear, and maintaining consistently high IOP for several weeks to 11 months (Pelzel et al., 2006; Quigley and

[1]Department of Ophthalmology, Guangdong Provincial Key Laboratory of Malignant Tumor Epigenetics and Gene Regulation, Sun Yat-Sen Memorial Hospital, Sun Yat-Sen University, Guangzhou, China

[2]Guangdong Provincial Key Laboratory of Laboratory Animals, Guangdong Laboratory Animals Monitoring Institute, Guangdong Laboratory Animals Monitoring Institute, Guangzhou, China

[3]Department of Sports Medicine, The Affiliated Hospital of Qingdao University, Qingdao, China

[4]Guangdong Provincial Key Laboratory of Malignant Tumor Epigenetics and Gene Regulation, Medical Research Center, Sun Yat-Sen Memorial Hospital, Sun Yat-Sen University, Guangzhou, China

[5]These authors contributed equally

[6]Lead contact

*Correspondence: lanyq@mail.sysu.edu.cn (Y.L.), suyy36@mail.sysu.edu.cn (Y.S.)

https://doi.org/10.1016/j.isci.2022.104149

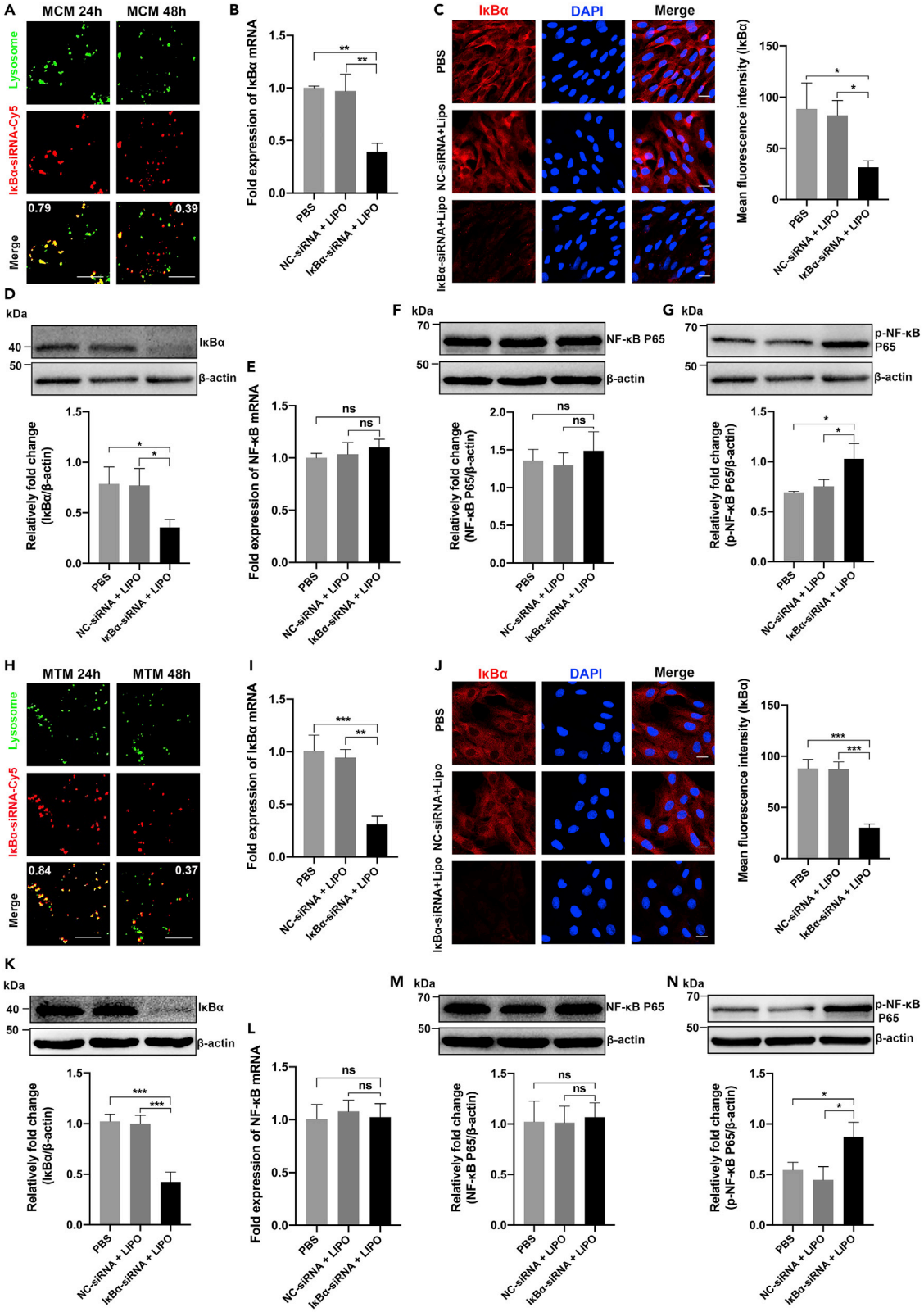
A
MCM 24h
MCM 48h
Lysosome
IκBα-siRNA-Cy5
Merge
0.79
0.39
B
Fold expression of IκBα mRNA
PBS
NC-siRNA + LIPO
IκBα-siRNA + LIPO
C
IκBα
DAPI
Merge
PBS
NC-siRNA+Lipo
IκBα-siRNA+Lipo
Mean fluorescence intensity (IκBα)
D
kDa
IκBα
β-actin
Relatively fold change (IκBα/β-actin)
E
Fold expression of NF-κB mRNA
F
NF-κB P65
Relatively fold change (NF-κB P65/β-actin)
G
p-NF-κB P65
Relatively fold change (p-NF-κB P65/β-actin)
H
MTM 24h
MTM 48h
0.84
0.37
I
J
K
L
M
N
ns

Figure 1. Knockdown of IκBα and activation of NF-κB P65 in MCM and MTM cells after IκBα-siRNA transfection 48 h in the blank, negative control, and experimental groups

(A and H) Colocalization of IκBα-siRNA-Cy5 with the lysosomes in MCM and MTM cells at 24 and 48 h incubation. PCC values were displayed in white. Scale bar 20 μm.

(B and I) qPCR showed the mRNA expression of IκBα in MCM and MTM cells (n = 3).

(C and J) IF and mean fluorescence intensity analysis showed the expression of IκBα in MCM and MTM cells (n = 3). Scale bar 20 μm.

(D and K) WB and mean gray value analysis showed the expression of IκBα in MCM and MTM cells (n = 3).

(E and L) qPCR showed the mRNA expression of NF-κB P65 in MCM and MTM cells (n = 3).

(F, G, M and N) WB and mean gray value analysis showed the expression of NF-κB P65 and phospho-NF-κB P65 (p-NF-κB P65) in MCM and MTM cells (n = 3).

The data of (B–G) and (I–N) are presented as the mean ± SD. *p < 0.05, **p < 0.01, ***p < 0.001, ns not significant by one-way ANOVA.

Hohman, 1983; Tu et al., 2019). Given the necessity in developing a potent anti-glaucomatous drug, it is better to establish a nonhuman primate model of COHT and that LP-induced COHT model is more ideal.

Eyes, which have a clear anatomy, relative immune privilege, and relatively isolated compartment that limits systemic exposure, are a good target for RNAi therapy. RNAi-based mechanisms, especially the use of small interfering RNAs (siRNAs), have been used in research to treat several chronic diseases and have shown promising results for ocular diseases, including glaucoma (Cassidy et al., 2021; Diaz-Canestro et al., 2021; Feng et al., 2021; Nguyen et al., 2012; Ray et al., 2017). Due to their high susceptibility to enzyme hydrolysis, rapid removal from circulatory system siRNA, virus vectors or nanoparticle carriers are needed. Notably, the silenced gene has to be re-synthesized in order to recover its biological activity after siRNA treatment, so the siRNA compound strategies have much more prolonged effect compared with commercial pharmaceutical products (Behlke 2006; Liu et al., 2009; Lu et al., 2005). Matrix metalloproteinases (MMPs)-mediated extracellular matrix (ECM) remodeling in the TM and ciliary muscle (CM) reduces outflow resistance in the conventional (trabecular) and unconventional (uveoscleral) outflow pathways, and helps maintain IOP homeostasis (Acott et al., 2021; Bradley et al., 1998; De Groef et al., 2016; De Groef et al., 2013; O'Callaghan et al., 2017; Toris et al., 2008; Weinreb et al., 2020). The secretion of MMPs depends on the activation of NF-κB in vascular smooth muscle and macrophages (Bond et al., 2001; Chase et al., 2002). In TM and human ciliary muscle (HCM) cells, upregulation of MMPs has been also shown to be mediated by NF-κB (Lan et al., 2009; Porter et al., 2012). NF-κB remains inactive when bound to IκB in the cytoplasm. Phosphorylation of IκB results in its ubiquitination and degradation, which releases NF-κB for nuclear translocation and stimulates the transcription of genes (Ramkumar et al., 2011). In addition, downregulation of IκBα plays a crucial role in reducing IOP in rats (Zeng et al., 2020). However, whether and how IκB-siRNA working in MTM and/or MCM of COHT nonhuman primate, and whether it further achieves the goal of long-lasting IOP-lowering are unknown.

In this study, we investigated whether IκBα-siRNA could inhibit the synthesis of IκBα *in vitro* and *in vivo*, and then increase the secretion of MMPs by activating NF-κB to play a long-term and potent role in reducing IOP in nonhuman primates COHT models.

RESULTS

Characterization of MCM and MTM cells

Primary MCM and MCM cells were successively harvested at least three times to produce three cell lines that were used in the following experiments. The primary MCM cells were validated in immunofluorescence using two markers: α-smooth muscle actin (α-SMA) (a variant of actin expressed specifically in smooth muscle cells) and desmin (a muscle-specific intermediate filament protein) (Hutchinson et al., 2010; Tamm et al., 1991; Zhao et al., 2003). Our cultured MCM cells showed both α-SMA and desmin immunoreactivity in all cells (Figure S1A). No fluorescence was detected in the negative control (NC) group (secondary antibodies only) both in MCM and MTM cells (Figure S1B). Besides, a number of criteria, including the expression of RSPO4 (spreading throughout the TM but not surrounding tissues (Patel et al., 2020)), neuron-specific enolase (NSE), fibronectin (FN), and collagen type IV (Col IV) (Fan et al., 2019; Guo et al., 2012; Mao et al., 2013; Patel et al., 2020), as well as Dex-induced increased expression of myocilin (MYOC) (Clark et al., 2001; Fan et al., 2019; Fingert et al., 2001), were used to characterize isolated MTM cells. We first studied the expression RSPO4, NSE, FN, and Col IV in MTM cells by immunofluorescence. All four proteins were expressed in our MTM cells (Figure S1C). Furthermore, the MTM cells showed increased expression of MYOC following induction by Dex (p = 0.0026) (Figure S1D).

IκBα-siRNA colocalizes with lysomoes *in vitro*

As shown in the merged images in Figure 1A, the Pearson's correlation coefficient (PCC) value of the fluorescent signals of IκBα-siRNA-Cy5 and lysosomes was up to 0.79 and 0.84 in the primary MCM cells and

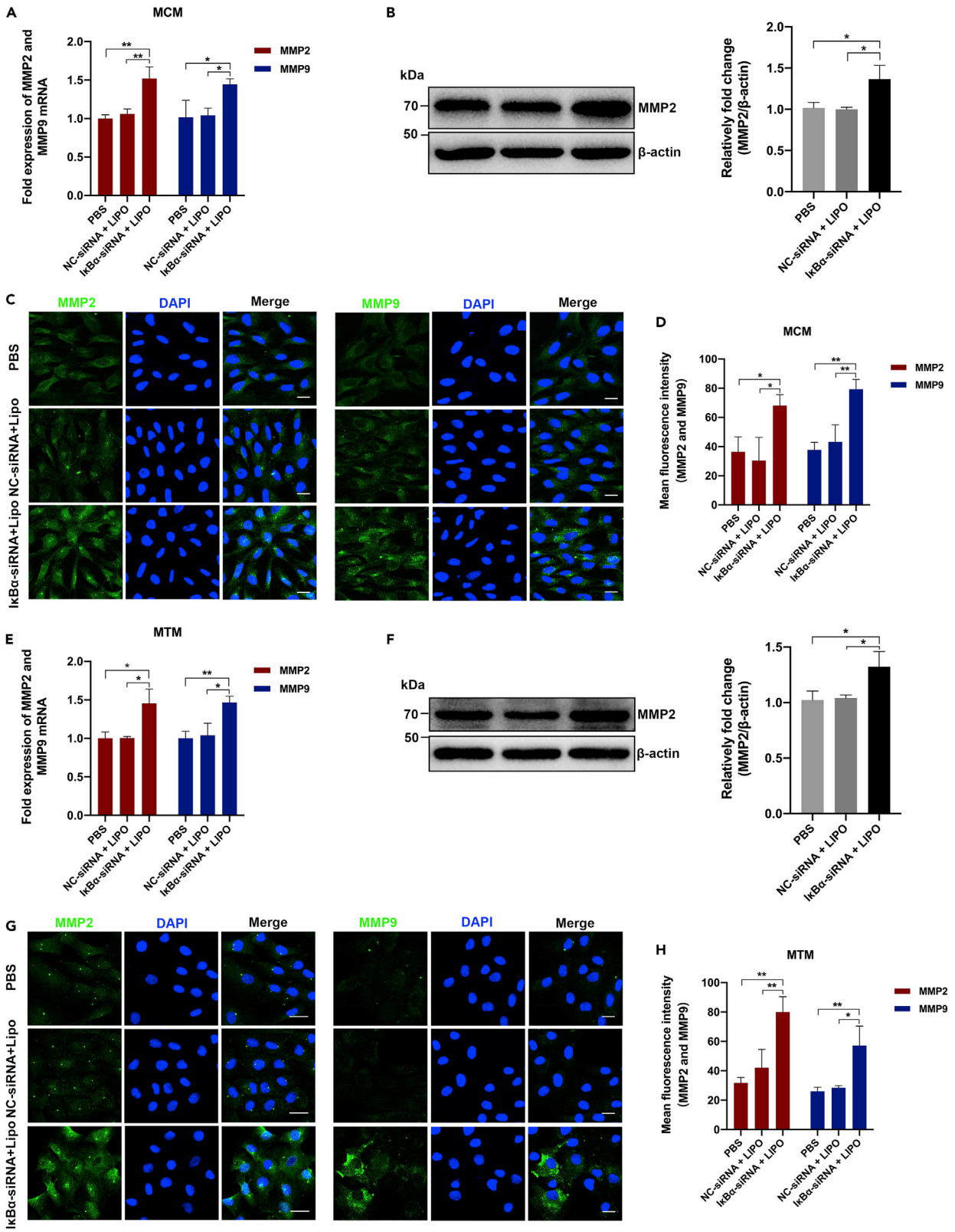
A
MCM
Fold expression of MMP2 and MMP9 mRNA
MMP2
MMP9
PBS
NC-siRNA + LIPO
IκBα-siRNA + LIPO
B
kDa
70
50
MMP2
β-actin
Relatively fold change (MMP2/β-actin)
C
MMP2
DAPI
Merge
MMP9
PBS
NC-siRNA+Lipo
IκBα-siRNA+Lipo
D
MCM
Mean fluorescence intensity (MMP2 and MMP9)
E
MTM
F
G
H
MTM

Figure 2. Protein and mRNA expression of MMPs in MCM and MTM cells after knockdown of IκBα for 48 h in the blank, negative control, and experimental groups

(A and E) qPCR showed the mRNA expression of MMP2 and MMP9 in MCM and MTM cells (n = 3).

(B and F) WB and mean gray value analysis showed the expression of MMP2 in MCM and MTM cells (n = 3).

(C, D, G and H) IF and mean fluorescence intensity analysis showed the expression of MMP2 and MMP9 in MCM and MTM cells (n = 3). Scale bar 20 μm. The data of (A, B, D) and (E, F, H) are represented as the mean ± SD. *p < 0.05, **p < 0.01, ***p < 0.001, ns not significant by one-way ANOVA.

MTM cells separately after incubation for 24 h, providing additional quantitative confirmation of the obviously strong colocalization of IκBα-siRNA and lysosomes. In comparison, the PCC value decreased to 0.39 and 0.37 in MCM cells and MTM cells after 48 h, respectively. These results demonstrated great consistency with that observed by confocal imaging experiments, the IκBα-siRNA located primarily in lysosomes after 24 h incubation, while it was gradually released from lysosomes after 48 h incubation (Figures 1A and 1H).

IκBα-siRNA transfection knockdowns IκBα and activates NF-κB P65 *in vitro*

As described previously, we identified primary MCM cells and MTM cells, and screened the optimal sequence and concentration of IκBα-siRNA to inhibit the expression of IκBα (Ou et al., 2020). IκBα mRNA expression was significantly decreased in the experimental group compared with the blank and negative control groups after transfection of IκBα-siRNA for 48 h in the primary MCM cells (p = 0.0006) (Figure 1B) and in the MTM cells (p = 0.0004) (Figure 1I). Likewise, the decrease in IκBα protein expression was statistically significant in the experimental group compared with the blank and negative control groups in primary MCM cells by immunofluorescence (IF) (p = 0.0124) and western blotting (WB) (p = 0.0178) analysis (Figures 1C and 1D), while similar trend obtained by IF (p < 0.0001) and WB (p = 0.0002) analysis in primary MTM cells (Figures 1J and 1K). In addition, we found that although the mRNA and protein expression of NF-κBp65 did not change significantly both in primary MCM and MTM cells by qPCR (p = 0.3765, p = 0.7751) and WB (p = 0.5078, p = 0.9190) analysis (Figures 1E and 1F and 1L and lM), the protein expression of phospho-NF-κBp65 increased after transfection of IκBα-siRNA both in the primary MCM and MTM cells by WB analysis (p = 0.0125, p = 0.0119) (Figures 1G and 1N).

Knockdown of IκBα upregulates the expression of MMPs *in vitro*

To further investigate the effects of IκBα on the expression of MMPs in the primary MCM and MTM cells, we verified it at the mRNA and protein levels.

qPCR analysis revealed the upregulated mRNA expression of MMP2 (p = 0.0013) and MMP9 (p = 0.0189) compared with the blank and negative control groups after knockdown of IκBα for 48 h in the primary MCM cells (Figure 2A). We found similar regulatory effects in the primary MTM cells (MMP2, p = 0.0049; MMP9, p = 0.0046) (Figure 2E).

WB analysis showed the upregulated protein expression of MMP2 (p = 0.0092) compared with the blank and negative control groups after knockdown of IκBα for 48 h in the primary MCM cells (Figure 2B). We also found similar regulatory effects in the primary MTM cells (p = 0.0122) (Figure 2F).

IF analysis supported the upregulated protein expression of MMP2 (p = 0.0158) and MMP9 (p = 0.0017) compared with the blank and negative control groups after knockdown of IκBα for 48 h in the primary MCM cells (Figures 2C and 2D), the similar regulatory effects was found in the primary MTM cells (MMP2, p = 0.0020; MMP9, p = 0.0047) (Figures 2G and 2H).

LP induces stable and long-lasting COHT in rhesus monkeys

Six eyes from three monkey models successfully established COHT (Figure 3A), and two eyes from one monkey were set as blank controls. The baseline IOP was 13.50 ± 2.51 mmHg, which was similar to those of previous studies (Lin et al., 2021; Pasquale et al., 2021; Quigley and Hohman, 1983; Tu et al., 2019). There was no elevated IOP in any eye after the first LP, and fluctuating IOP appeared after the second LP. Inflammation of the anterior chamber occurred in the early stage after LP. Two eyes maintained stable high IOP during the observation period of 2 months after the second LP, and the mean IOP reached 45.90 ± 8.25 mmHg. After the inflammation subsided, fluctuating IOP decreased to normal levels in four eyes, stable COHT was obtained in the remaining four eyes after the third LP, and the mean IOP reached 49.35 ± 7.15 mmHg during the observation period of 1 month (Figure 3B).

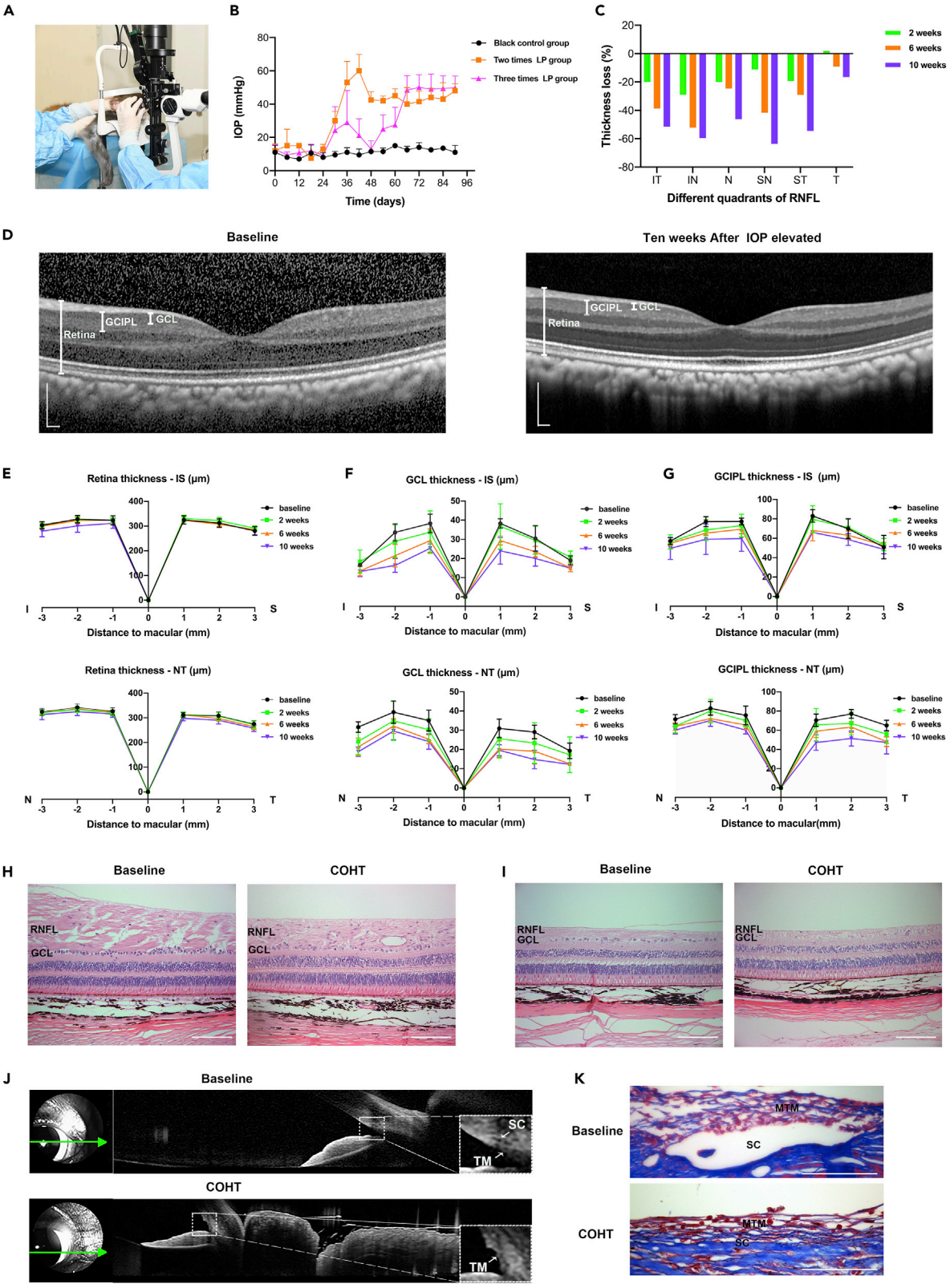
A
B
IOP (mmHg)
Time (days)
Black control group
Two times LP group
Three times LP group
C
Thickness loss (%)
Different quadrants of RNFL
IT
IN
N
SN
ST
T
2 weeks
6 weeks
10 weeks
D
Baseline
Ten weeks After IOP elevated
Retina
GCIPL
GCL
E
Retina thickness - IS (μm)
Retina thickness - NT (μm)
F
GCL thickness - IS (μm)
GCL thickness - NT (μm)
G
GCIPL thickness - IS (μm)
GCIPL thickness - NT (μm)
baseline
2 weeks
6 weeks
10 weeks
Distance to macular (mm)
I
S
N
T
H
Baseline
COHT
RNFL
GCL
I
Baseline
COHT
RNFL
GCL
J
Baseline
COHT
SC
TM
K
Baseline
COHT
MTM
SC

Figure 3. Establishment of COHT in rhesus monkeys

(A) A representative operation photo of LP in a rhesus monkey.

(B) Time course of IOP changes in six eyes after LP compared to two blank eyes.

(C) The thickness of the peripapillary RNFL at baseline and IOP remained high for 2, 6, and 10 weeks in the infratemporal (IT), infranasal (IN), nasal (N), supranasal (SN), supratemporal (ST), and temporal (T) regions.

(D) SD-OCT scanning of the macula was performed before LP and measured again after 10 weeks of elevated IOP in the same eye. Scale bar 200 μm.

(E–G) The GCL/GCIPL/retina thickness at distances of 1, 2, and 3 mm from the macular fovea at baseline and the IOP remained high for 2, 6, and 10 weeks in the inferior (I), superior (S), nasal (N), and temporal (T) regions. See also Tables S1A–S1C.

(H and I) H&E staining of paraffin sections of blank control eyes and COHT eyes in the peripapillary and peripheral retina. Scale bar 100 μm.

(J) Representative OCT scanned images at the anterior chamber corner before and after three LPs.

(K) Masson staining of paraffin sections of blank control eyes and COHT eyes in the TM. Scale bar 100 μm. See also Figure S2.

The thickness analysis of the peripapillary retinal nerve fiber layer (RNFL) via SD-OCT scanning showed that the thickness of the infranasal (IN) (reduced by 29.02%), infratemporal (IT) (reduced by 20.0%), nasal (N) (reduced by 19.99%), and supratemporal (ST) (reduced by 19.41%) became obvious thinner two weeks after IOP increased. During the following two-month observation period, when the IOP remained high and stable, the RNFL thickness in all quadrants gradually became thinner to varying degrees, especially in the IN (reduced by 59.62%), IT (reduced by 51.48%), supranasal (SN) (reduced by 63.61%), ST (reduced by 54.43%), and N (reduced by 46.23%) (Figure 3C).

According to the statistics of retinal thickness around the macular fovea scanned by SD-OCT, it was found that the thickness of ganglion cell layer (GCL) and ganglion cell inner plexiform layer (GCIPL) was obvious thinner than baseline after 10 weeks of elevated IOP in a long-term observed monkey (Figure 3D). There was no significant change in macular retinal thickness after 10 weeks of elevated IOP (Figure 3E and Table S1A). The scan of the macular fovea showed that the thickness of GCL and GCIPL decreased in four quadrants (inferior, superior, nasal, and temporal) after IOP increased. IOP began to rise over 2 weeks, the thickness of GCL and GCIPL in the nasal quadrant which was 3 mm away from the macular fovea, that was, the area close to the optic disc, became thinner. During the next two months, IOP remained high, and the thickness of the GCL and GCIPL in the four quadrants around the macular fovea became thinner and gradually reduced with time. Except for similar temporal changes, the GCL was more sensitive to the increase in IOP than the GCIPL (Figures 3F, 3G, Tables S1B and S1C). The changes in the GCL and GCIPL in the macula and peripapillary RNFL were consistent with the changes in glaucoma observed by SD-OCT.

H&E staining of paraffin sections showed that the RNFL and GCL around the optic disc in the COHT group were reduced compared with those in the control group (Figure 3H). The same changes were found in the peripheral retina (Figure 3I).

In vivo, anterior OCT scan showed the patent *Schlemm*'s Canal (SC) and smooth surface of the TM in the anterior chamber angle before LP, while collapsed SC and compact TM could be observed after LP (Figure 3J). Also, Masson staining of paraffin sections showed detailed damage to the TM structure after LP. The destroyed collagen structure of TM and collapsed SC were observed (Figures 3K and S2).

Intracameral injection of IκBα-siRNA has a potent and long-lasting efficacy

The effects of the intracameral injection of 90–100 μg IκBα-siRNA on the IOP of one COHT eye compared with one COHT eye without any drug intervention are shown in Figure S3A. IκBα-siRNA lowered the IOP in the monkey eye from Day 2 to Day 28 after injection compared with the baseline and blank control eye, especially from Day 4 to Day 16. However, mild corneal edema, anterior chamber exudation, and cells were observated in the eye injected with 90–100 μg IκBα-siRNA on the first day after injection, which were improved on the Day 4 after the operation (Figure S3B).

The effects of the intracameral injection of 5–10 μg IκBα-siRNA or 5–10 μg NC-siRNA on the IOP of COHT monkeys are shown in Figure 4B. IκBα-siRNA was injected in the left eye of two monkeys with COHT as the experimental group, while NC-siRNA was injected in the right eye as the negative control group. The pretreatment IOP of the four eyes from two monkeys involved was 44 ± 9.17 mmHg (5–10 μg NC-siRNA) and 42.55 ± 6.56 mmHg (5–10 μg IκBα-siRNA). Impressively, the dose of 5–10 μg showed similar IOP-lowering effect to 90–100μg. IκBα-siRNA (5–10 μg) lowered the IOP in the eyes of monkey with COHT from Day 2 to Day 28 after injection compared with the baseline and negative control group. The effect of IOP lowering was very significant, especially from Day 4 to Day 16. The IOP decreased to 14.36 ± 5.15 mmHg, and the

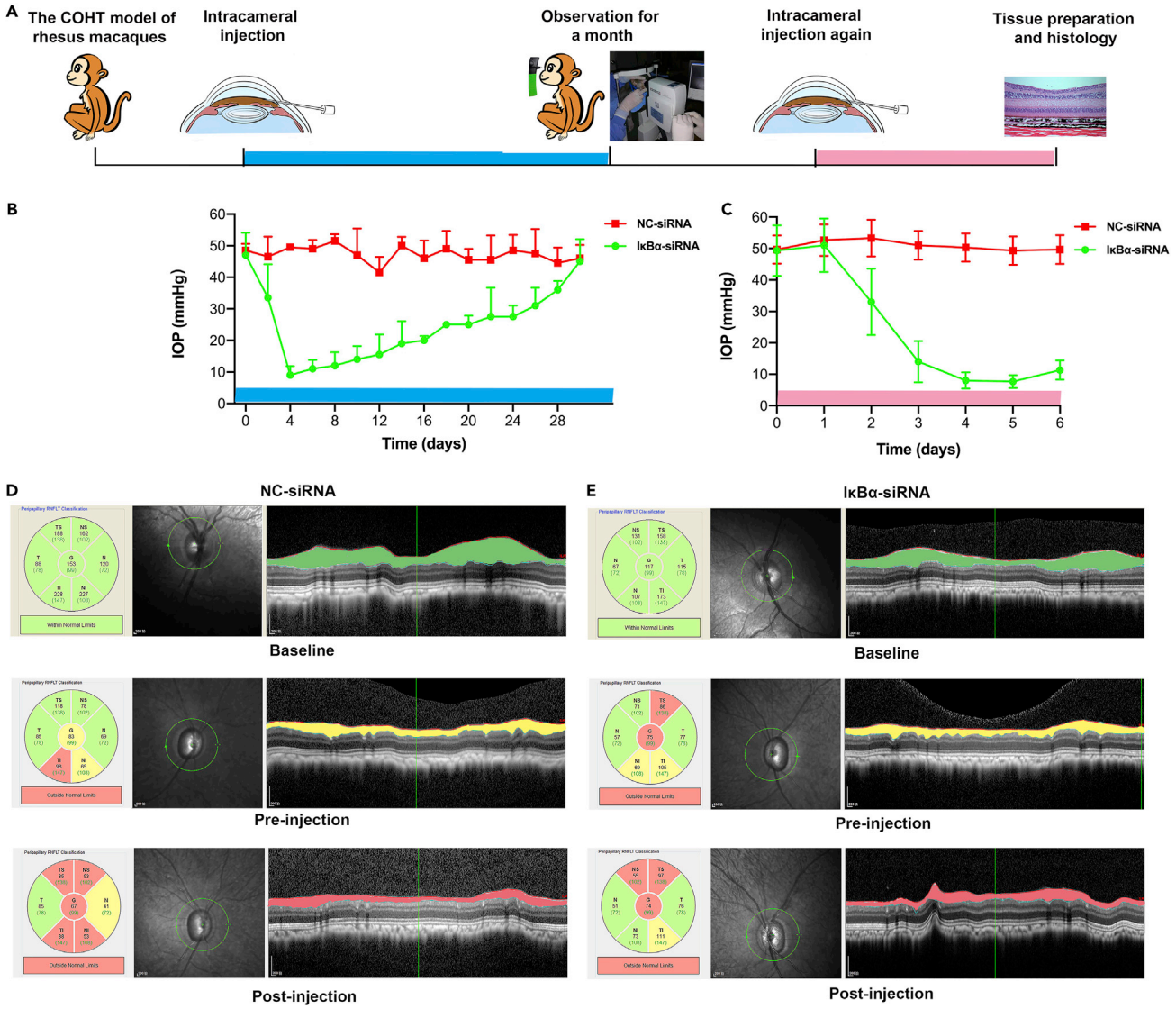

Figure 4. Efficacy of 5–10 μg IκBα-siRNA intracameral injection

(A) Flow chart of rhesus monkey *in vivo*.

(B) Time course of IOP changes in COHT eyes after 5–10 μg IκBα-siRNA, or 5–10 μg NC-siRNA intracameral injection separately (n = 2).

(C) Time course of IOP changes in COHT eyes after 5–10 μg IκBα-siRNA or 5–10 μg NC-siRNA intracameral injection again (n = 3).

(D and E) SD-OCT images showing the progression of peripapillary RNFL in the negative control group (5–10 μg NC-siRNA) and in the experimental group (5–10 μg IκBα-siRNA) from baseline to COHT and finally to 1 month after injection in one rhesus monkey. Peripapillary RNFL in different time is distinguished by green, yellow, and red respectively.

mean IOP decreased by 66.25% compared to the baseline. In the following 12 days, the effect of IκBα-siRNA still persisted, the IOP was 28.67 ± 5.42 mmHg, and the mean IOP decreased by 32.62% compared to the baseline. Overall, the mean IOP from Day 2 to Day 28 after injection was 21.86 ± 9.42 mmHg, which decreased by 48.63% compared to the baseline. However, the mean IOP from Day 2 to Day 28 after NC-siRNA injection was 47.25 ± 4.63 mmHg. And the IOP in the NC-siRNA-treated eyes did not show obvious changes post treatment compared to the baseline.

Three monkeys with COHT eyes were injected with 5–10 μg IκBα-siRNA in the left eye and 5–10 μg NC-siRNA in the right eye again (Figure 4A). A slit-lamp biomicroscope and the IOP were monitored every day after the second injection. The effect of reducing IOP began on the second day as before. The maximum effect of reducing IOP was observated on the fourth and fifth days (7.83 ± 2.14 mmHg), which

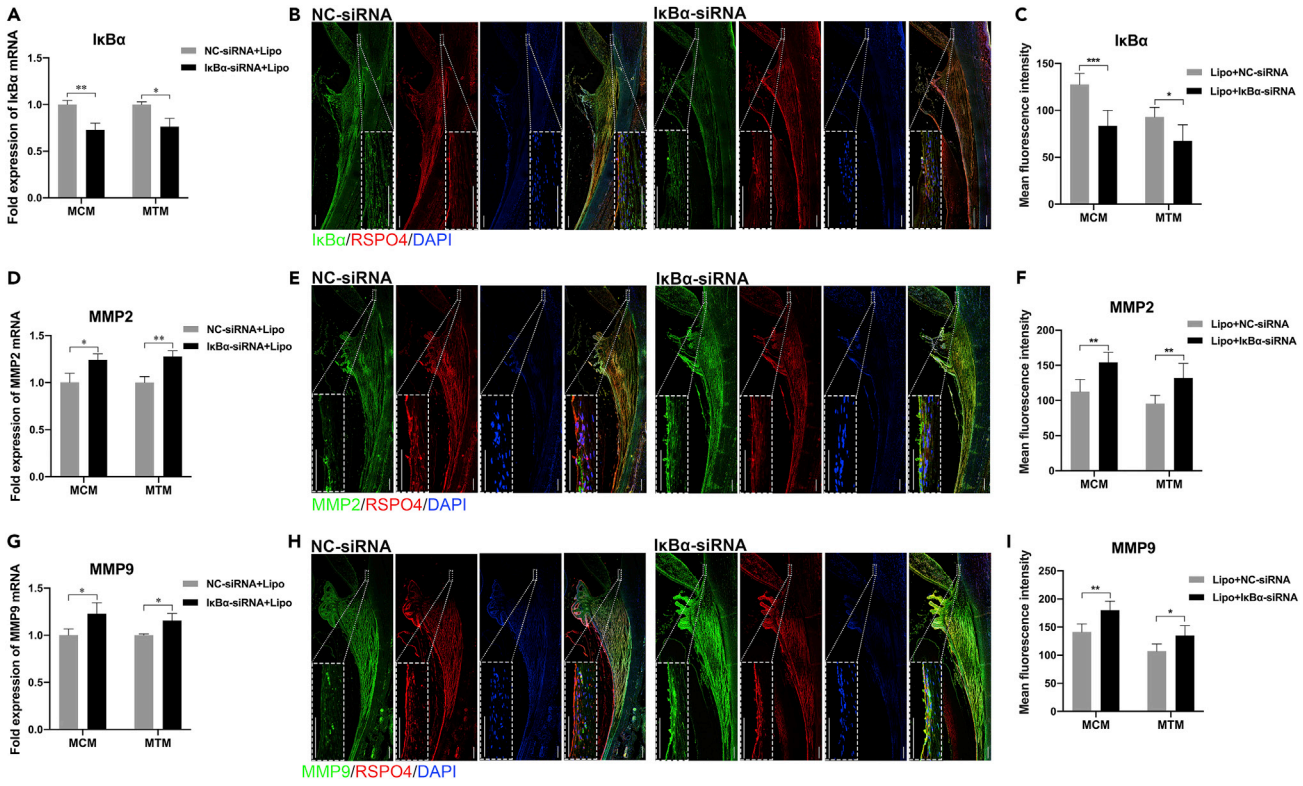

Figure 5. Proteins and mRNA expression of IκBα, MMP2, and MMP9 *in vivo*

(A, D and G) qPCR showed the mRNA expression of IκBα, MMP2, and MMP9 in the MCM and MTM after intracameral injection for 6 days in the negative control and experimental groups (n = 1).

(B, E and H) IκBα, MMP2, and MMP9 expression in the MCM and MTM after intracameral injection for 6 days in the negative control and experimental groups by IF. Scale bar 100 μm.

(C, F and I) Fluorescence intensity analysis of IκBα, MMP2, and MMP9 in the MCM and MTM (n = 2). The data of (A, C, D, F, G, I) are presented as the mean ± SD. *p < 0.05, **p < 0.01, ***p < 0.001, ns not significant using Student's *t* test.

was 84.13% (41.50 mmHg) lower than the baseline (49.33 mmHg) (Figure 4C). The effect and trend of reducing IOP were similar to the previous treatment.

We showed the progression of peripapillary RNFL in the negative control group (5–10 μg NC-siRNA) and in the experimental group (5–10 μg IκBα-siRNA) from one monkey with COHT (Figures 4D and 4E). Before any intervention, the peripapillary RNFL thickness of both eyes was in the normal range. The RNFL thickness became thinner to some extent after 6 weeks of COHT. One month after intracameral injection, the IOP in the negative control group was maintained at a high level (50.21 ± 2.46 mmHg), and the thickness of the peripapillary RNFL became obvious thinner, while the IOP in the experimental group was maintained at 22.43 ± 11.77 mmHg. And the peripapillary RNFL thickness continued to thin, but it was not as severe as that in the negative control group.

Downregulation of IκBα upregulates MMPs of the MCM and MTM *in vivo*

We investigated the changes in IκBα, MMP2, and MMP9 proteins and mRNA of the eyes in the negative control group and in the experimental group by IF and qPCR. As shown in Figure 5, mRNA expression of IκBα was significantly decreased in the MCM and MTM after IκBα-siRNA intracameral injection compared to that in the NC-siRNA group (MCM, p = 0.0050; MTM, p = 0.0116) (Figure 5A), and the protein expression of IκBα showed similar trend both in the MCM and MTM (MCM, p = 0.0003; MTM, p = 0.0106) (Figures 5B and 5C). As expected, the mRNA expression increasing trends of MMP2, MMP9 in the MCM, and MTM were consistent with the expression *in vitro* (MMP2 in the MCM, p = 0.0222; MMP9 in the MCM, p = 0.0407; MMP2 in the MTM, p = 0.0051; MMP9 in the MTM, p = 0.0254) (Figures 5D and 5G). In addition, the protein expression of MMP2 and MMP9 in the MCM and MTM also showed an increasing

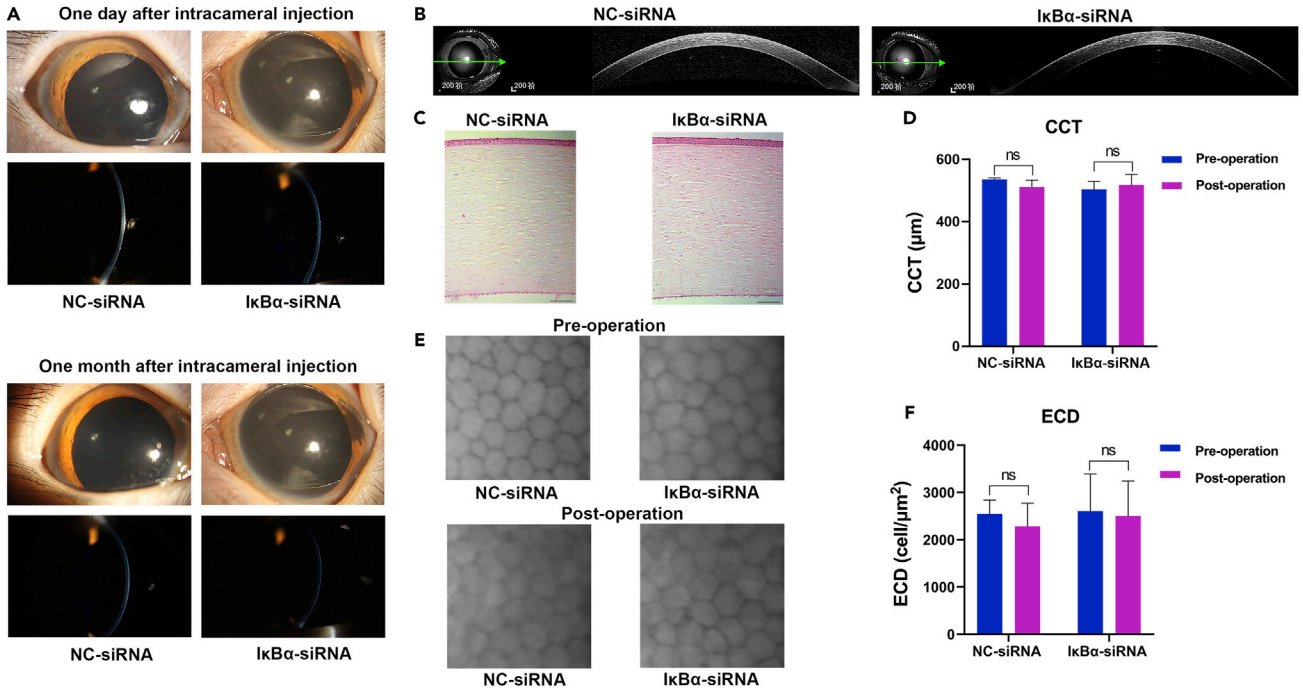

Figure 6. Safety of 5–10 μg IκBα-siRNA intracameral injection

(A) Representative images of slit-lamp examination of the monkey eyes at different time points, including the general status on the first day and 1 month after the operation in the negative control and experimental groups.

(B) Anterior segment OCT scan of cornea 1 month after intracameral injection in the negative control and experimental groups.

(C) H&E staining images of the central cornea in experimental and negative control eyes. Scale bar 100 μm.

(D) Central corneal thickness (CCT) obtained via anterior segment OCT scan before and 1 month after intracameral injection in the two groups (n = 3).

(E) Representative images of corneal endothelium pictures in the negative control and experimental groups before and after treatment by specular microscopy. See also Table S2.

(F) Endothelial cell density (ECD) before and 1 month after intracameral injection in the two groups (n = 3). The data of (D) and (F) are represented as the mean ± SD. *p < 0.05, **p < 0.01, ***p < 0.001, ns not significant using Student's *t* test.

trend after IκBα-siRNA intracameral injection by IF (MMP2 in the MCM, p = 0.0011; MMP9 in the MCM, p = 0.0013; MMP2 in the MTM, p = 0.0040; MMP9 in the MTM, p = 0.0106) (Figures 5E, 5F, 5H and 5I). An increased protein expression of MMP2 and MMP9 in the MCM and MTM might promote ECM turnover *in vivo*, which lowered the IOP by reducing aqueous humor outflow resistance.

Obvious eyes' adverse reactions do not occur after IκBα-siRNA intracameral injection

There was no corneal edema or serious inflammatory reaction in the negative control eye (5–10 μg NC-siRNA) during the observation period of one month after intracameral injection. Mild aqueous cells occurred in eyes injected with 5–10 μg IκBα-siRNA, which were absorbed in following 2 days. Slit-lamp examination recorded the general conditions of the eyes on the first day and 1 month after intracameral injection (Figure 6A). There was no significant change in the anterior segment of the eyes both in the negative control group (5–10 μg NC-siRNA) and the experimental group (5–10 μg IκBα-siRNA) one month after intracameral injection.

Anterior segment OCT scan showed that there was no obvious difference in central corneal thickness (CCT) between the two groups 1 month after intracameral injection (Figure 6B). And there was no significant difference in CCT before and 1 month after intracameral injection both in the negative control group (p = 0.1302) and in the experimental group (p = 0.5790) (Figure 6D). H&E staining of paraffin sections showed corneal structure changes between the two groups' eyes (Figure 6C). There was no edema or thickening of the corneal stroma and no obvious abnormality of the corneal structure.

The ECD of both eyes was counted by specular microscopy before and 1 month after intracameral injection. There was no obvious abnormality in the morphology of the corneal endothelium before treatment of

either eye, and there was no significant change one month after injection in the two groups ($p = 0.4661$, $p = 0.8759$) (Figures 6E, 6F and Table S2).

DISCUSSION

Our previous studies showed that the IκB/NF-κB signaling pathway plays an important role in the expression of MMP2 in HCM cells and in the CM of rats (Lan et al., 2009; Zeng et al., 2020). Inhibition of IκBα expression by IκBα-siRNA led to translocation of NF-κBp65 from the cytoplasm to the nucleus, increased secretion of MMP2 in HCM cells (Lan et al., 2009). In addition to the above changes, IOP of rats decreased after IκBα-siRNA intracameral injection (Zeng et al., 2020). In the present study, we found that with the knockdown of IκBα after RNAi, NF-κBp65 was activated, and the secretion of MMP2 and MMP9 increased in the primary MCM and MTM cells. Moreover, IκBα-siRNA intracameral injection showed a significant and long-lasting IOP-lowering effect *in vivo* with a well-characterized LP-induced nonhuman primate model of COHT, and the expression of the above associated mRNAs and proteins was also confirmed in the MCM and MTM tissues of rhesus monkeys.

To simulate human glaucoma, we chose LP-induced COHT in rhesus monkeys as the disease model to verify the effect of reducing the IOP of IκBα-siRNA. Previous studies have found that the COHT model achieved IOP >30 mmHg after LP, and the maintenance time varies from weeks to months due to individual differences (Pelzel et al., 2006; Quigley and Hohman, 1983; Tu et al., 2019). In our study, the IOP was stable at 47.63 ± 7.81 mmHg after two to three LPs within 3 weeks to 2 months of the observation period, and there was no significant decrease in the negative treatment control group during the follow-up period. As expected, in our results, histopathology showed that the TM structure was damaged, and most SC collapsed after LP. In addition, the loss of RFNL and GCL thickness are hallmarks of neurodegenerative processes in glaucoma (Beykin et al., 2021). In the present study, decreased thickness of the peripapillary RNFL, GCL, and GCIPL of the macula in COHT was detected 2 weeks after IOP elevation. Not only peripapillary RNFL but also GCL and GCIPL of the macula have high sensitivity in the early diagnosis of glaucoma. As expected, the thickness of the peripapillary RNFL, GCL, and GCIPL of the macula became thinner in the following two months when the IOP remained stable, which was consistent with the performance of glaucoma (Beykin et al., 2021; Hood et al., 2013). Taken overall, the COHT rhesus monkey model induced by LP is highly consistent with human glaucoma in the changes of IOP and retina.

Topical anti-glaucoma drugs are the most common treatment strategy to reduce IOP, but the difficulties of limited treatment effects and short action times in approved anti-glaucoma drugs are hard to overcome due to topical application. The longer-lasting effect compared to commercial pharmaceutical products is the main advantage of siRNA strategies. The latest RNAi treatment for glaucoma has mainly focused on the Rho/ROCK pathway and β2 adrenergic receptors et al. RhoA and ROCKs are distributed in the outflow pathway, including TM, JCT, and SC, which reduce IOP by increasing aqueous outflow through TM (Goldhagen et al., 2012). Intracameral injection of LIPO-mediated RhoA-siRNA reduced IOP by approximately 26% for 4 days in DEX-treated mouse eyes and reduced IOP by approximately 16% for 1 day in normal mouse eyes (Liu et al., 2012). Self-complementary adeno-associated virus serotype 2 carrying the mutated RhoA (scAAV2.dnRhoA) injection prevented elevation of nocturnal IOP for at least 4 weeks (Borrás et al., 2015). Lentiviral vector-mediated expression of exoenzyme C3 caused the IOP-lowering effect to reach a peak of 11.83 ± 2.51 mmHg at Day 3 post delivery, and $\triangle$IOP gradually decreased from Day 7 to Day 42 and then was maintained at approximately 4 mmHg from 49 to 91 days in monkey eyes by inactivating Rho (Tan et al., 2019). Similar to Rho/ROCK pathway-targeted siRNA, SYL040012 is a siRNA designed to specifically silence β2 adrenergic receptor and reduce IOP by approximately 20% for 167 h in rabbits after administration over a 4-day period by decreasing the production of aqueous humor (Martínez et al., 2014). Topical instillation of β2 adrenergic receptor siRNA induced a reduction in IOP of $30 \pm 5\%$ for 78–120 h in rabbits (Loma et al., 2018). Besides, ZO-1 and tricellulin siRNA-targeting SC endothelial tight junctions enhancing outflow facility showed an average IOP decrease of approximately 2 mmHg in DEX-treated mice eyes after 48 h intracameral injection, representing twice that measured in normotensive controls (approximately 1 mmHg) (Cassidy et al., 2021). Intracameral injection of adenovirus vector encoding wild-type human metalloproteinase 1 (AdhGRE. MMP1) quickly induced a maximum hypotensive effect both in normal and steroid-induced ocular hypertension sheep eyes within 48 h, and the IOP-lowering effect lasted for at least 15 days (Gerometta et al., 2010). Viral vectors are the preferred system for gene delivery because of their higher *in vivo* transfection efficiency. It shows a longer-lasting effect due to being more persistent with being self-complementarity. However, viral gene delivery systems have disadvantages related to limited payload capacity, potential immunogenicity, and no known pathogenicity (Dang

et al., 2017; Gardlík et al., 2005; Glover et al., 2005). In our study, the mean IOP was reduced by 20.69 mmHg (48.63%) on the Day 2 to Day 28 after injection, and the IOP even decreased by 28.19 mmHg(66.25%) on the Day 4 to Day 16 in monkeys with COHT, which showed a more potent and long-lasting effect of reducing IOP with nonviral vectors than the above studies.

Activation of the NF-κB signaling pathway is often contributed to the occurrence of inflammation and glaucoma (Vernazza et al., 2020). Under chronic stress conditions, the ER accumulates reactive oxygen species and promotes oxidative stress-induced TM damage (Anholt and Carbone, 2013; Cullinan and Diehl, 2006). Damaged ER activates inflammatory processes via NF-κB, mitochondrial changes, and enhanced TM cell apoptosis, which lead to elevated IOP (Rao et al., 2004). Hernandez et al. showed that NF-κB was necessary for TGFβ2-induced ECM production and ocular hypertension (Hernandez et al., 2020), whereas the level of MMPs was not detected and the molecular mechanisms by which NF-κB upregulates the ECM is not fully understood. However, several studies had indicated the opposite conclusion. NF-κB mediated ECM degradation in osteoarthritis cartilage and skin (Hussain et al., 2018; Kaur et al., 2015). In addition, the DEX-induced reduction in MMP-2 and MMP-9 secretion was prevented by NF-κB activation in HTM cells (Mohd Nasir et al., 2020). Besides, it had been demonstrated that the mechanism of IOP lowering by prostaglandin analogs (PGAs, i.e., the first-line treatment for open-angle glaucoma) involves the increasement of MMPs in TM and CM, and tissue remodeling that enhances conventional and unconventional outflow (Toris et al., 2008; Weinreb et al., 2020). Promoting MMPs expression, which is responsible for ECM remodeling by activated NF-κB in the initial stage of glaucoma, is meaningful for lowering IOP (Saccà et al., 2020). Just as PGAs were initially found to have IOP-lowering effects, in 1977, Camras et al. found that low doses of topical PGAs decreased IOP (Camras et al., 1977; Eakins 1977). In contrast, large quantities of PGAs infused into animal eyes led to ocular inflammation with breakdown of the blood-aqueous barrier. However, appropriate amount of PGAs have emerged as the most potent IOP-lowering topical medication and are rarely accompanied by uveitis. A statistical study showed that the incidences of uveitis and cystoid macular edema among PGAs users were very rare at 62/28232 (0.22%) and 25/28232 (0.09%), respectively (Hu et al., 2020). In the current study, corneal edema and inflammatory reactions only occurred in the anterior segment of the eye 1–4 days after intracameral injection of 90–100 μg IκBα-siRNA without an obvious increase in IOP, and corneal edema and inflammatory reactions completely disappeared during our observation. What's more, IκBα-siRNA (5–10 μg) showed only a slight inflammatory reaction (mild aqueous cells) 1–3 days after intracameral injection, and there was no significantly increased IOP compared with the negative control group. Interestingly, it showed a similar effect of reducing IOP in the following 1 month. Therefore, the effect of IκBα-siRNA on reducing IOP is worth affirming, and we speculate that the observation of inflammation may be related to the dose, and the optimal dose needs to be further studied.

In conclusion, IκBα-siRNA increased the secretion of MMP2 and MMP9 by activating the NF-κB signaling pathway *in vitro* and *in vivo*. And IκBα-siRNA with nonviral vectors showed long-term and potent effects of reducing IOP in monkeys with COHT. Therefore, IκBα-siRNA may become a new and promising therapeutic approach for the treatment of glaucoma.

Limitations of the study

In this study, we verified the definite IOP-lowering effect of IκBα-siRNA in monkeys with COHT by promoting the expressions of MMP2 and MMP9 in MCM and MTM. However, the specific effect of IκBα-siRNA on the aqueous humor outflow resistance in the trabecular meshwork and uveoscleral pathways needs further investigation.

STAR★METHODS

Detailed methods are provided in the online version of this paper and include the following:

- KEY RESOURCES TABLE
- RESOURCE AVAILABILITY
  - Lead contact
  - Materials availability
  - Data and code availability
- EXPERIMENTAL MODEL AND SUBJECT DETAILS
  - Animal
  - Isolation and culture of primary MCM and MTM cells

SUPPLEMENTAL INFORMATION

Supplemental information can be found online at https://doi.org/10.1016/j.isci.2022.104149.

ACKNOWLEDGMENTS

This study was supported by grants from the National Natural Science Foundation of China (No. 81570845) and the Sun Yat-sen Clinical Research Cultivation Project (No.SYS-C-201705).

AUTHOR CONTRIBUTIONS

Conception and design: YL, YS, DS, ZZ, and RZ. Performed the research and data collection: DS, XL, ZZ, FY, SH, YL, and ZY. Data analysis and interpretation: DS, BW, and ZZ. Funding: YL. Writing–original draft: DS. Writing–review & editing: YS, ZZ, and YL.

DECLARATION OF INTERESTS

The authors declare no competing interests.

Received: December 23, 2021
Revised: February 28, 2022
Accepted: March 20, 2022
Published: April 15, 2022

REFERENCES

Acott, T.S., Vranka, J.A., Keller, K.E., Raghunathan, V., and Kelley, M.J. (2021). Normal and glaucomatous outflow regulation. Prog. Retin. Eye Res. *82*, 100897.

Anholt, R.R., and Carbone, M.A. (2013). A molecular mechanism for glaucoma: endoplasmic reticulum stress and the unfolded protein response. Trends Mol. Med. *19*, 586–593.

Baudouin, C., Kolko, M., Melik-Parsadaniantz, S., and Messmer, E.M. (2021). Inflammation in Glaucoma: from the back to the front of the eye, and beyond. Prog. Retin. Eye Res. *83*, 100916.

Behlke, M.A. (2006). Progress towards in vivo use of siRNAs. Mol. Ther. *13*, 644–670.

Beykin, G., Norcia, A.M., Srinivasan, V.J., Dubra, A., and Goldberg, J.L. (2021). Discovery and clinical translation of novel glaucoma biomarkers. Prog. Retin. Eye Res. *80*, 100875.

Bond, M., Chase, A.J., Baker, A.H., and Newby, A.C. (2001). Inhibition of transcription factor NF-kappaB reduces matrix metalloproteinase-1, -3 and -9 production by vascular smooth muscle cells. Cardiovasc. Res. *50*, 556–565.

Borrás, T., Buie, L.K., Spiga, M.G., and Carabana, J. (2015). Prevention of nocturnal elevation of intraocular pressure by gene transfer of dominant-negative RhoA in rats. JAMA Ophthalmol. *133*, 182–190.

Bradley, J.M., Vranka, J., Colvis, C.M., Conger, D.M., Alexander, J.P., Fisk, A.S., Samples, J.R., and Acott, T.S. (1998). Effect of matrix metalloproteinases activity on outflow in perfused human organ culture. Invest. Ophthalmol. Vis. Sci. *39*, 2649–2658.

Camras, C.B., Bito, L.Z., and Eakins, K.E. (1977). Reduction of intraocular pressure by prostaglandins applied topically to the eyes of conscious rabbits. Invest. Ophthalmol. Vis. Sci. *16*, 1125–1134.

Cassidy, P.S., Kelly, R.A., Reina-Torres, E., Sherwood, J.M., Humphries, M.M., Kiang, A.S., Farrar, G.J., O'Brien, C., Campbell, M., Stamer, W.D., et al. (2021). siRNA targeting Schlemm's canal endothelial tight junctions enhances outflow facility and reduces IOP in a steroid-induced OHT rodent model. Mol. Ther. Methods Clin. Dev. *20*, 86–94.

Chase, A.J., Bond, M., Crook, M.F., and Newby, A.C. (2002). Role of nuclear factor-kappa B activation in metalloproteinase-1, -3, and -9 secretion by human macrophages in vitro and rabbit foam cells produced in vivo. Arterioscler. Thromb. Vasc. Biol. *22*, 765–771.

Chen, H., Wei, X., Cho, K.S., Chen, G., Sappington, R., Calkins, D.J., and Chen, D.F. (2011). Optic neuropathy due to microbead-induced elevated intraocular pressure in the mouse. Invest. Ophthalmol. Vis. Sci. *52*, 36–44.

Clark, A.F., Steely, H.T., Dickerson, J.E., Jr., English-Wright, S., Stropki, K., McCartney, M.D., Jacobson, N., Shepard, A.R., Clark, J.I., Matsushima, H., et al. (2001). Glucocorticoid induction of the glaucoma gene MYOC in human

and monkey trabecular meshwork cells and tissues. Invest. Ophthalmol. Vis. Sci. *42*, 1769–1780.

Cullinan, S.B., and Diehl, J.A. (2006). Coordination of ER and oxidative stress signaling: the PERK/Nrf2 signaling pathway. Int. J. Biochem. Cell Biol. *38*, 317–332.

Dang, Y., Loewen, R., Parikh, H.A., Roy, P., and Loewen, N.A. (2017). Gene transfer to the outflow tract. Exp. Eye Res. *158*, 73–84.

De Groef, L., Andries, L., Siwakoti, A., Geeraerts, E., Bollaerts, I., Noterdaeme, L., Etienne, I., Papageorgiou, A.P., Stalmans, I., Billen, J., et al. (2016). Aberrant collagen composition of the trabecular meshwork results in reduced aqueous humor drainage and elevated IOP in MMP-9 null mice. Invest. Ophthalmol. Vis. Sci. *57*, 5984–5995.

De Groef, L., Van Hove, I., Dekeyster, E., Stalmans, I., and Moons, L. (2013). MMPs in the trabecular meshwork: promising targets for future glaucoma therapies? Invest. Ophthalmol. Vis. Sci. *54*, 7756–7763.

Diaz-Canestro, C., Puspitasari, Y.M., Liberale, L., Guzik, T.J., Flammer, A.J., Bonetti, N.R., Wüst, P., Constantino, S., Paneni, F., Akhmedov, A., et al. (2021). MMP-2 knockdown blunts age-dependent carotid stiffness by decreasing elastin degradation and augmenting eNOS activation. Cardiovasc. Res. cvab300. https://doi.org/10.1093/cvr/cvab300.

Eakins, K.E. (1977). Prostaglandin and non-prostaglandin mediated breeakdown of the blood-aqueous barrier. Exp. Eye Res. *25*, 483–498.

Evans, D.T., and Silvestri, G. (2013). Nonhuman primate models in AIDS research. Curr. Opin. HIV AIDS *8*, 255–261.

Fan, Y., Guo, L., Wei, J., Chen, J., Sun, H., and Guo, T. (2019). Effects of salidroside on trabecular meshwork cell extracellular matrix expression and mouse intraocular pressure. Invest. Ophthalmol. Vis. Sci. *60*, 2072–2082.

Feng, N., Liang, L., Fan, M., Du, Y., Chen, C., Jiang, R., Yu, D., Yang, Y., Zhang, M., Deng, L., et al. (2021). Treating autoimmune inflammatory diseases with an siERN1-nanoprodrug that mediates macrophage polarization and blocks Toll-like receptor signaling. ACS Nano *15*, 15874–15891.

Fingert, J.H., Clark, A.F., Craig, J.E., Alward, W.L., Snibson, G.R., McLaughlin, M., Tuttle, L., Mackey, D.A., Sheffield, V.C., and Stone, E.M. (2001). Evaluation of the myocilin (MYOC) glaucoma gene in monkey and human steroid-induced ocular hypertension. Invest. Ophthalmol. Vis. Sci. *42*, 145–152.

Gardlík, R., Pálffy, R., Hodosy, J., Lukács, J., Turna, J., and Celec, P. (2005). Vectors and delivery systems in gene therapy. Med. Sci. Monit. *11*, Ra110–121.

Garway-Heath, D.F., Crabb, D.P., Bunce, C., Lascaratos, G., Amalfitano, F., Anand, N., Azuara-Blanco, A., Bourne, R.R., Broadway, D.C., Cunliffe, I.A., et al. (2015). Latanoprost for open-angle glaucoma (UKGTS): a randomised, multicentre, placebo-controlled trial. Lancet *385*, 1295–1304.

Gerometta, R., Spiga, M.G., Borrás, T., and Candia, O.A. (2010). Treatment of sheep steroid-induced ocular hypertension with a glucocorticoid-inducible MMP1 gene therapy virus. Invest. Ophthalmol. Vis. Sci. *51*, 3042–3048.

Glover, D.J., Lipps, H.J., and Jans, D.A. (2005). Towards safe, non-viral therapeutic gene expression in humans. Nat. Rev. Genet. *6*, 299–310.

Goldhagen, B., Proia, A.D., Epstein, D.L., and Rao, P.V. (2012). Elevated levels of RhoA in the optic nerve head of human eyes with glaucoma. J. Glaucoma *21*, 530–538.

Guo, M.S., Wu, Y.Y., and Liang, Z.B. (2012). Hyaluronic acid increases MMP-2 and MMP-9 expressions in cultured trabecular meshwork cells from patients with primary open-angle glaucoma. Mol. Vis. *18*, 1175–1181.

Hernandez, H., Roberts, A.L., and McDowell, C.M. (2020). Nuclear factor-kappa beta signaling is required for transforming growth factor Beta-2 induced ocular hypertension. Exp. Eye Res. *191*, 107920.

Hood, D.C., Raza, A.S., de Moraes, C.G., Liebmann, J.M., and Ritch, R. (2013). Glaucomatous damage of the macula. Prog. Retin. Eye Res. *32*, 1–21.

Hu, J., Vu, J.T., Hong, B., and Gottlieb, C. (2020). Uveitis and cystoid macular oedema secondary to topical prostaglandin analogue use in ocular hypertension and open angle glaucoma. Br. J. Ophthalmol. *104*, 1040–1044.

Hussain, S., Sun, M., Min, Z., Guo, Y., Xu, J., Mushtaq, N., Heng, L., Huang, H., Zhao, Y., Yuan, Y., et al. (2018). Down-regulated in OA cartilage, SFMBT2 contributes to NF-κB-mediated ECM degradation. J. Cell Mol. Med. *22*, 5753–5758.

Hutchinson, A.J., Coons, S.C., Chou, C.L., Xu, W., Stamer, W.D., Woodward, D.F., and Regan, J.W. (2010). Induction of angiogenic immediate early genes by activation of FP prostanoid receptors in cultured human ciliary smooth muscle cells. Curr. Eye Res. *35*, 408–418.

Kasetti, R.B., Maddineni, P., Patel, P.D., Searby, C., Sheffield, V.C., and Zode, G.S. (2018). Transforming growth factor β2 (TGFβ2) signaling plays a key role in glucocorticoid-induced ocular hypertension. J. Biol. Chem. *293*, 9854–9868.

Kaur, S., Kizoulis, M., Fantasia, J., Oddos, T., Bigot, N., Galera, P., Tucker-Samaras, S., Leyden, J.J., and Southall, M.D. (2015). 4-Hexyl-1,3-phenylenediol, a nuclear factor-κB inhibitor, improves photodamaged skin and clinical signs of ageing in a double-blinded, randomized controlled trial. Br. J. Dermatol. *173*, 218–226.

Lan, Y.Q., Zhang, C., Xiao, J.H., Zhuo, Y.H., Guo, H., Peng, W., and Ge, J. (2009). Suppression of IkappaBalpha increases the expression of matrix metalloproteinase-2 in human ciliary muscle cells. Mol. Vis. *15*, 1977–1987.

Lin, K.H., Tran, T., Kim, S., Park, S., Stout, J.T., Chen, R., Rogers, J., Yiu, G., Thomasy, S., and Moshiri, A. (2021). Advanced retinal imaging and ocular parameters of the rhesus macaque eye. Transl. Vis. Sci. Technol. *10*, 7.

Liu, Q., Wu, K., Qiu, X., Yang, Y., Lin, X., and Yu, M. (2012). siRNA silencing of gene expression in trabecular meshwork: RhoA siRNA reduces IOP in mice. Curr. Mol. Med. *12*, 1015–1027.

Liu, X., Rasmussen, C.A., Gabelt, B.T., Brandt, C.R., and Kaufman, P.L. (2009). Gene therapy targeting glaucoma: where are we? Surv. Ophthalmol. *54*, 472–486.

Loma, P., Guzman-Aranguez, A., de Lara, M.J.P., and Pintor, J. (2018). Beta2 adrenergic receptor silencing change intraocular pressure in New Zealand rabbits. J. Optom. *11*, 69–74.

Lu, P.Y., Xie, F., and Woodle, M.C. (2005). In vivo application of RNA interference: from functional genomics to therapeutics. Adv. Genet. *54*, 117–142.

Mao, W., Liu, Y., Wordinger, R.J., and Clark, A.F. (2013). A magnetic bead-based method for mouse trabecular meshwork cell isolation. Invest. Ophthalmol. Vis. Sci. *54*, 3600–3606.

Martínez, T., González, M.V., Roehl, I., Wright, N., Pañeda, C., and Jiménez, A.I. (2014). In vitro and in vivo efficacy of SYL040012, a novel siRNA compound for treatment of glaucoma. Mol. Ther. *22*, 81–91.

Mohd Nasir, N.A., Agarwal, R., Krasilnikova, A., Sheikh Abdul Kadir, S.H., and Iezhitsa, I. (2020). Effect of trans-resveratrol on dexamethasone-induced changes in the expression of MMPs by human trabecular meshwork cells: involvement of adenosine A(1) receptors and NFkB. Eur. J. Pharmacol. *887*, 173431.

Nguyen, Q.D., Schachar, R.A., Nduaka, C.I., Sperling, M., Klamerus, K.J., Chi-Burris, K., Yan, E., Paggiarino, D.A., Rosenblatt, I., Aitchison, R., et al. (2012). Evaluation of the siRNA PF-04523655 versus ranibizumab for the treatment of neovascular age-related macular degeneration (MONET Study). Ophthalmology *119*, 1867–1873.

O'Callaghan, J., Cassidy, P.S., and Humphries, P. (2017). Open-angle glaucoma: therapeutically targeting the extracellular matrix of the conventional outflow pathway. Expert Opin. Ther. Targets *21*, 1037–1050.

Ou, Z., Zeng, R., Lin, Y., Zhang, S., Alzogool, M., Zeng, P., and Lan, Y. (2020). In vitro screening and transfection concentration optimization of cynomolgus monkey IκBα-siRNA. J. Ophthalmol. *2020*, 1848540.

Pasquale, L.R., Gong, L., Wiggs, J.L., Pan, L., Yang, Z., Wu, M., Yang, Z., Chen, D.F., and Zeng, W. (2021). Development of primary open angle glaucoma-like features in a rhesus macaque colony from southern China. Transl. Vis. Sci. Technol. *10*, 20.

Patel, G., Fury, W., Yang, H., Gomez-Caraballo, M., Bai, Y., Yang, T., Adler, C., Wei, Y., Ni, M., Schmitt, H., et al. (2020). Molecular taxonomy of human ocular outflow tissues defined by single-cell transcriptomics. Proc. Natl. Acad. Sci. U S A. *117*, 12856–12867.

Pelzel, H.R., Schlamp, C.L., Poulsen, G.L., Ver Hoeve, J.A., Nork, T.M., and Nickells, R.W. (2006). Decrease of cone opsin mRNA in experimental ocular hypertension. Mol. Vis. *12*, 1272–1282.

Porter, K.M., Epstein, D.L., and Liton, P.B. (2012). Up-regulated expression of extracellular matrix remodeling genes in phagocytically challenged trabecular meshwork cells. PLoS One *7*, e34792.

Quigley, H.A., and Hohman, R.M. (1983). Laser energy levels for trabecular meshwork damage in the primate eye. Invest. Ophthalmol. Vis. Sci. *24*, 1305–1307.

Ramkumar, V., Jhaveri, K.A., Xie, X., Jajoo, S., and Toth, L.A. (2011). Nuclear factor κB and adenosine receptors: biochemical and behavioral profiling. Curr. Neuropharmacol. *9*, 342–349.

Rao, R.V., Ellerby, H.M., and Bredesen, D.E. (2004). Coupling endoplasmic reticulum stress to the cell death program. Cell Death Differ. *11*, 372–380.

Rasmussen, C.A., and Kaufman, P.L. (2005). Primate glaucoma models. J. Glaucoma *14*, 311–314.

Ray, K.K., Landmesser, U., Leiter, L.A., Kallend, D., Dufour, R., Karakas, M., Hall, T., Troquay, R.P., Turner, T., Visseren, F.L., et al. (2017). Inclisiran in patients at high cardiovascular risk with elevated LDL cholesterol. N. Engl. J. Med. *376*, 1430–1440.

Rodrigo, M.J., Garcia-Herranz, D., Subias, M., Martinez-Rincón, T., Mendez-Martínez, S., Bravo-Osuna, I., Carretero, A., Ruberte, J., Garcia-Feijoo, J., Pablo, L.E., et al. (2021). Chronic glaucoma using biodegradable microspheres to induce intraocular pressure elevation. Six-month follow-up. Biomedicines *9*, 682.

Roelfsema, P.R., and Treue, S. (2014). Basic neuroscience research with nonhuman primates: a small but indispensable component of biomedical research. Neuron *82*, 1200–1204.

Saccà, S.C., Tirendi, S., Scarfì, S., Passalacqua, M., Oddone, F., Traverso, C.E., Vernazza, S., and Bassi, A.M. (2020). An advanced in vitro model to assess glaucoma onset. Altex *37*, 265–274.

Samsel, P.A., Kisiswa, L., Erichsen, J.T., Cross, S.D., and Morgan, J.E. (2011). A novel method for the induction of experimental glaucoma using magnetic microspheres. Invest. Ophthalmol. Vis. Sci. *52*, 1671–1675.

Stewart, W.C., Magrath, G.N., Demos, C.M., Nelson, L.A., and Stewart, J.A. (2011). Predictive value of the efficacy of glaucoma medications in animal models: preclinical to regulatory studies. Br. J. Ophthalmol. *95*, 1355–1360.

Tamm, E., Flügel, C., Baur, A., and Lütjen-Drecoll, E. (1991). Cell cultures of human ciliary muscle: growth, ultrastructural and immunocytochemical characteristics. Exp. Eye Res. *53*, 375–387.

Tan, J., Liu, G., Zhu, X., Wu, Z., Wang, N., Zhou, L., Zhang, X., Fan, N., and Liu, X. (2019). Lentiviral vector-mediated expression of exoenzyme C3 Transferase lowers intraocular pressure in monkeys. Mol. Ther. *27*, 1327–1338.

Tomalka, J.A., Pelletier, A.N., Fourati, S., Latif, M.B., Sharma, A., Furr, K., Carlson, K., Lifton, M., Gonzalez, A., Wilkinson, P., et al. (2021). The transcription factor CREB1 is a mechanistic driver of immunogenicity and reduced HIV-1 acquisition following ALVAC vaccination. Nat. Immunol. *22*, 1294–1305.

Toris, C.B., Gabelt, B.T., and Kaufman, P.L. (2008). Update on the mechanism of action of topical prostaglandins for intraocular pressure reduction. Surv. Ophthalmol. *53*, S107–S120.

Tu, S., Li, K., Ding, X., Hu, D., Li, K., and Ge, J. (2019). Relationship between intraocular pressure and retinal nerve fibre thickness loss in a monkey model of chronic ocular hypertension. Eye (Lond) *33*, 1833–1841.

Varma, R., Lee, P.P., Goldberg, I., and Kotak, S. (2011). An assessment of the health and economic burdens of glaucoma. Am. J. Ophthalmol. *152*, 515–522.

Vernazza, S., Tirendi, S., Bassi, A.M., Traverso, C.E., and Saccà, S.C. (2020). Neuroinflammation in primary open-angle glaucoma. J. Clin. Med. *9*, 3172.

Weber, A.J., and Harman, C.D. (2005). Structure-function relations of parasol cells in the normal and glaucomatous primate retina. Invest. Ophthalmol. Vis. Sci. *46*, 3197–3207.

Wegener, D., Oh, D.Q.P., Lukaß, H., Böer, M., and Kreiter, A.K. (2021). Blood analysis of laboratory Macaca mulatta used for neuroscience research: investigation of long-term and cumulative effects of implants, fluid control, and laboratory procedures. eNeuro *8*, ENEURO.0284-21.2021.

Weinreb, R.N., Robinson, M.R., Dibas, M., and Stamer, W.D. (2020). Matrix metalloproteinases and glaucoma treatment. J. Ocul. Pharmacol. Ther. *36*, 208–228.

Zeng, R., Li, J., Gong, H., Luo, J., Li, Z., Ou, Z., Zhang, S., Yang, L., and Lan, Y. (2020). Hyperbranched cationic glycogen derivative-mediated IκBα gene silencing regulates the uveoscleral outflow pathway in rats. Biomed. Res. Int. *2020*, 8206849.

Zhao, X., Pearson, K.E., Stephan, D.A., and Russell, P. (2003). Effects of prostaglandin analogues on human ciliary muscle and trabecular meshwork cells. Invest. Ophthalmol. Vis. Sci. *44*, 1945–1952.

Zode, G.S., Sharma, A.B., Lin, X., Searby, C.C., Bugge, K., Kim, G.H., Clark, A.F., and Sheffield, V.C. (2014). Ocular-specific ER stress reduction rescues glaucoma in murine glucocorticoid-induced glaucoma. J. Clin. Invest. *124*, 1956–1965.

STAR★METHODS

KEY RESOURCES TABLE

REAGENT or RESOURCE	SOURCE	IDENTIFIER
Antibodies		
rabbit monoclonal anti-IκBα	Cell Signaling Technology	Cat# 4812S; RRID: AB_10694416
rabbit monoclonal anti-NF-κB P65	Cell Signaling Technology	Cat# 8242S; RRID: AB_10859369
rabbit monoclonal anti-phospho-NF-κB P65	Cell Signaling Technology	Cat# 3033S; RRID: AB_331284
mouse monoclonal anti-MMP2	Invitrogen	Cat# 436000; RRID: AB_1501404
rabbit monoclonal anti-β-actin	Cell Signaling Technology	Cat# 8457S; RRID: AB_10950489
rabbit monoclonal anti-α-smooth muscle actin (α-SMA)	Bioss	Cat# bsm-33187M;RRID: AB_2910163
goat polyclonal anti-desmin	R&D Systems	Cat# AF3844; RRID: AB_2092419
rabbit anti-RSPO4	Bioss	Cat# bs-18878R; RRID: AB_2910164
rabbit polyclonal anti-NSE	Bioss	Cat# bs-1027R; RRID: AB_10855053
rabbit anti-FN	Bioss	Cat# bs-4859R; RRID: AB_2910165
goat polyclonal anti-Col IV	Millipore	Cat# AB769; RRID: AB_92262
mouse monoclonal anti-MYOC	Santa Cruz Biotechnology	Cat# sc-137233; RRID: AB_2148737
mouse monoclonal anti-IκBα	Cell Signaling Technology	Cat# 4812T RRID; AB_390781
mouse monoclonal anti-MMP9	R&D Systems	Cat# MAB936, RRID; AB_2282047
Chemicals, peptides, and recombinant proteins		
Lipofectamine® RNAiMAX	Invitrogen	Cat# 13778150
LysoTracker® Green DND-26	Invitrogen	Cat# L7526
Fetal bovine serum	Gibco	Cat# 10099-141
Mounting medium with DAPI - Aqueous, Fluoroshield	Abcam	Cat# ab104139
Experimental models: Cell lines		
Rhesus monkey ciliary muscle cells and trabecular meshwork cells	This study	N/A
Experimental models: Organisms/strains		
Rhesus monkey	Guangdong Laboratory Animals Monitoring Institute	N/A
Oligonucleotides		
ACTB forward primer:5′-AGATCAAGATCATTGCTCCTCCTG-3′	This study	N/A
ACTB reverse primer:5′-TCACAGTCCGCCTAGAAGCA-3′	This study	N/A
IκBα forward primer:5′-CTGGTGTCGCTCCTGTTGAAGTG-3′	This study	N/A
IκBα reverse primer:5′-TGTCATAGCTCTCCTCATCCTCACTC-3′	This study	N/A
NF-κB forward primer:5′-TCAGCGCATCCAGACGAACAAC-3′	This study	N/A
NF-κB reverse primer:5′-AAGCAGAGCCGCACAGCATTC-3′	This study	N/A
MMP2 forward primer:5′-CACCTACACCAAGAACTTCCGTCTG-3′	This study	N/A
MMP2 reverse primer:5′-GTGCCAAGGTCAATGTCAGGAGAG-3′	This study	N/A
MMP9 forward primer:5′-TCTGCCAGGACCGCTTCTACTG-3′	This study	N/A
MMP9 reverse primer:5′-GCAGGATGTCATAGGTCACGTAGC-3′	This study	N/A
Software and algorithms		
GraphPad Prism 8.0	GraphPad Software	https://www.graphpad.com/
ImageJ	National Institute of Health	https://imagej.nih.gov/ij/
ZEN	Zeiss	https://www.zeiss.com/microscopy/us/products/microscope-software/zen.html

RESOURCE AVAILABILITY

Lead contact

Further information and requests for resources and reagents should be directed to and will be fulfilled by the lead contact, Yuqing Lan (lanyq@mail.sysu.edu.cn).

Materials availability

This study did not generate new unique reagents.

Data and code availability

All data reported in this paper will be shared by the lead contact upon request.

This paper does not report original code.

Any additional information required to reanalyze the data reported in this paper is available from the lead contact upon request.

EXPERIMENTAL MODEL AND SUBJECT DETAILS

Animal

All of the experiments were performed in accordance with the ARVO Statement for the Use of Animals in Ophthalmic and Vision Research. The study protocol was approved by the Ethics Committee of Guangdong Laboratory Animals Monitoring Institute (IACUC2020141). All efforts were made to limit the number of animals and to minimize animal suffering. The number of animals was in line with the principles of the 3Rs.

Four healthy male rhesus monkeys from the Guangdong Laboratory Animals Monitoring Institute, which were 3 to 4 years of age, were used in this study. All monkeys were housed in a room at 16~26°C and 40–70% humidity with a 12-h light-dark cycle. The monkeys' health was monitored daily by animal care staff and veterinary personnel.

Isolation and culture of primary MCM and MTM cells

Rhesus monkey (3 to 5 years old, sex balance) eyes were presented by Guangdong Laboratory Animals Monitoring Institute. Primary MCM cells and MTM cells were harvested at least three times. As described previously, we identified primary MCM cells and MTM cells, screened the optimal sequence and concentration of IκBα-siRNA to inhibit the expression of IκBα (Ou et al., 2020).The medium was composed of Dulbecco's modified Eagle's medium and Ham's F12 nutrient mixture (DMEM/F12, Gibco, USA) supplemented with 20% fetal bovine serum (FBS, Gibco, Australia), 1% penicillin-streptomycin (HyClone, USA), and 1 ng/mL recombinant human basic fibroblast growth factor (bFGF) (Gibco, USA). The cultures were incubated in a 37°C humidified incubator with 5% CO_2. The experiments were taken in the well-grown cells of 3-5 generations.

METHOD DETAILS

Identification of primary MCM and MTM cells

Primary cells were identified as MCM and MTM cells separately by immunofluorescence. In detail, the primary MCM cell cultures were validated by detecting the presence of α-SMA and desmin, while MTM cell cultures were certificated by detecting the expression of RSPO4, NSE, FN, and Col IV. Besides, cultured MTM cells stimulated with 100 nM Dex (Sigma-Aldrich Corp., USA) were added fresh every 3 days to the media for 10 days. The level of MYOC was analysed by immunofluorescence.

IκBα-siRNA transfection

Three pairs of siRNA against the IκBα gene and a pair of nonspecific control siRNA (NC-siRNA) were purchased from Guangzhou Ruibo Biotech Co., Ltd, China. Then, we screened the optimal one (5′-GCAC UUAGCCUCUAUCCAU-3′) and selected 10 nM as the optimal transfection concentration through the detection of transfection efficiency and cytotoxicity (Ou et al., 2020). Primary MCM cells and MTM cells were transfected with IκBα-siRNA or NC-siRNA and Lipofectamine® RNAiMAX Reagent (Invitrogen, USA) complex following the manufacturer's instructions. Both primary cells were divided into 3 groups: blank control (PBS), negative control group transfected with NC-siRNA and experimental group

transfected with IκBα-siRNA. Forty-eight hours after transfection, cells were collected for subsequent experiments.

Colocalization assays

To monitor whether IκBα-siRNA could be absorbed and released in MTM and MCM cells, colocalization with lysosome were examined after incubation for 24 hours and 48 hours, respectively. After transfection for 24 hours and 48 hours, LysoTracker Green DND-26 (ThermoFisher, USA) was added for 1 hour following the manufacturer's protocol. The images were taken under a laser confocal microscope (Zeiss LSM 880 with Airyscan, Germany). Pearson's correlation coefficient (PCC) was applied to describe colocation analysis by ImageJ software.

Real-time PCR (qPCR) analysis

Total RNA was extracted from each group *in vitro* and *in vivo* using an RNA Quick Purification kit (ESscience, China). RNA was reverse transcribed into cDNA using PrimeScript^{TM} RT Master Mix (Perfect Real Time) (Takara, Japan), and RT–PCR was performed with Green Premix Ex Taq II (Tli RNaseH Plus) (Takara, Japan). The related primers were designed and synthesized by Shanghai Biotech Co., Ltd. and were listed in the key resources table. The relative expression levels were calculated and analyzed using the $2^{-\Delta\Delta Ct}$ method. Among them, the experiment *in vitro* was repeated three times independently, and the results were used for subsequent statistical analysis. Besides, MTM and MCM tissues were collected from 1 eye of the negative control group and 1 eye of the experimental group, the experiment was repeated three times for subsequent statistical analysis.

Western blotting (WB)

Total protein was extracted from MCM and MTM cells with RIPA lysates (Epizyme, China) containing protease inhibitors (1:100; Epizyme, China) and nucleases (1:100; Hai-gene, China). The protein concentration of each sample was measured with a BCA Protein Assay Kit (Cwbio, China). After electrophoresis and transfer, the proteins were transferred to a 0.45-μm polyvinylidene fluoride (PVDF) membrane (Millipore, USA). Then, the membranes were blocked at room temperature (RT) for 15 minutes with a fast blocking solution (1:5; Epizyme, China) and incubated with selected primary antibodies at 4°C overnight. The membranes were washed in Tris-buffered saline containing 0.1% Tween 20 (1X TBST) and incubated with secondary antibodies for 1 hour at RT. Finally, the membranes were washed and imaged using the ChemiDocTM Touch Imaging System (Bio–Rad, USA). The following primary antibodies were used: rabbit anti-IκBα (1:5000; CST, USA), rabbit anti-NF-κB P65 (1:1000; CST, USA), rabbit anti-phospho-NF-κB P65 (1:1000; CST, USA), mouse anti-MMP2 (1:500; Invitrogen, USA), and rabbit anti-β-actin (1:10000; CST, USA). The secondary antibodies were HRP-labeled goat anti-rabbit IgG (1:5000; CST, USA) and HRP-labeled goat anti-mouse IgG (1:5000; CST, USA). The experiment was repeated three times independently. The gray value of each band was calculated and analyzed using ImageJ software.

Immunofluorescence (IF)

MCM and MTM cells were seeded on coverslips and transfected for 48 hours. They were fixed in a 4% paraformaldehyde solution (Bestbio, China) for 15 minutes and then permeabilized in 0.3% Triton X-100 (Solarbio, China) for 10 minutes at RT. Then, they were blocked with normal goat serum (Bioss, China) or 5% BSA for 1 hour at RT and incubated with selected primary antibodies at 4°C overnight. The coverslips were washed in TBST and incubated with secondary antibodies for 40 minutes at RT under dark conditions. After washing with TBST again, mounting medium with DAPI (Abcam, UK) was used, and images were taken by a Zeiss laser confocal microscope. The following primary antibodies were used: rabbit anti-α-SMA (1:100; Bioss, China), goat anti-desmin (1:100; R&D Systems, USA), rabbit anti-RSPO4 (1:100; Bioss, China), rabbit anti-NSE (1:100; Bioss, China), rabbit anti-FN (1:100; Bioss, China), goat anti-Col IV (1:200; Millipore, Germany), mouse anti-MYOC (1:100; Santa Cruz Biotechnology, USA), mouse anti-IκBα (1:100; CST, USA), mouse anti-MMP2 (1:100; Invitrogen, USA), mouse anti-MMP9 (1:100; R&D Systems, USA). The secondary antibodies were anti-mouse IgG (H + L), F(ab')$_2$ Fragment (Alexa Fluor® 555 Conjugate) (1:500; CST, USA) anti-rabbit IgG (H + L), F(ab')$_2$ Fragment (Alexa Fluor® 555 Conjugate) (1:500; CST, USA), and anti-mouse IgG (H + L), F(ab')$_2$ Fragment (Alexa Fluor® 488 Conjugate) (1:500; CST, USA), donkey anti-goat IgG (H + L) cross-adsorbed secondary antibody, Alexa Fluor 488 (1:500; Invitrogen, USA). The experiment was repeated three times independently, and the mean fluorescence intensities were calculated and analyzed by using ImageJ software.

Anesthesia

Rhesus monkeys were anesthetized with an intramuscular injection of ketamine hydrochloride (5 mg/kg) plus medetomidine (0.05 mg/kg). Topical corneal anesthesia was presented with oxybuprocaine hydrochloride eye drops (Santen Pharmaceutical Co., Ltd, Japan).

Establishment of a COHT monkey model and IOP measures

In this study, a COHT monkey model was established by destroying the TM with LP. Six eyes of 3 rhesus monkeys were treated with a TX532 laser photocoagulation instrument (Oculight TX; IRIDEX, USA). Pupils were sufficiently contracted with pilocarpine nitrate eye drops (Zhenrui ®; Bausch & Lomb, China) before LP. The laser parameters were as follows: 50 μm spot size, 0.5s duration, 800–1000 mW laser power and 150–250 spots. Photocoagulation of the middle trabecular meshwork in the entire circumference was completed, and each effective light spot was based on the generation of a bubble (Quigley and Hohman, 1983; Tu et al., 2019). Damage to the ciliary body band would be avoided as much as possible. Tobramycin and dexamethasone eye ointment (Tobradex® ; Alcon, USA) and Compound tropicamide eye drops (Zhuobian®; Sinqi, China) were used for alleviating the noninfectious inflammation for 3-7days.

All rhesus monkeys underwent a regular ophthalmological examination before and after LP, including IOP measurements, slit-lamp biomicroscopy, direct ophthalmoscopy, and OCT measurements. IOP was measured using the rebound tonometer (Tono Vet; Icare, Finland) according to the manufacturer's instructions. IOP measurements in this study were completed between 10 and 12 a.m. Each measurement of IOP was completed within 5 minutes after anesthesia took effect. The IOP of both eyes was measured three times, and the mean was calculated. The anterior segments of animals were regularly examined with a slit-lamp biomicroscope (KJ5DII, Suzhou Kangjie Medical Co., Ltd, China) and recorded, such as corneal clarity, anterior chamber cells and flares.

The baseline mean IOP of the rhesus monkeys was similar to that of humans (Lin et al., 2021; Pasquale et al., 2021). If the IOP was not consistently higher than 21 mmHg, additional LP was performed again at intervals of three weeks until stable IOP was obtained.

OCT measurements

Spectral-domain optical coherence tomography (SD-OCT; Heidelberg Engineering, Heidelberg, Germany) was applied to measure changes in the cornea and anterior chamber angle, especially central corneal thickness (CCT) and Schlemm's canal (SC).

SD-OCT was also applied to measure changes in the optic nerve head (ONH) and macula. The retinal nerve fiber layer (RNFL) thickness of the ONH and the retina, ganglion cell layer (GCL) and ganglion cell inner plexiform layer (GCIPL) thickness of the macula were measured. To minimize the risk of corneal dryness, artificial tears were applied during examination. Peripapillary RNFL thickness data were automatically obtained and recorded by the software. The retina, GCL and GCIPL thickness of the macula and CCT were manually measured by two researchers (D.F. Sun and Z.Y. Zhan), and the average value was taken.

Drug delivery to the anterior segment

There were 5–10 μg/90–100 μg IκBα-siRNA (2′OMe+5′Chol) (Guangzhou Ruibo Biotech Co., Ltd, China) or 5–10 μg NC-siRNA dissolved in 20 μL of sterile RNase free water; then, we added 3 μL of Lipofectamine® RNAiMAX Reagent(LIPO) and incubated at RT for 10 minutes. Intracameral injection was performed in six eyes of 3 monkeys with stable high IOP. The appropriate dose was selected according to the treatment results. Tobramycin eye ointment (Tobrex®, Alcon, USA) was topically administered to prevent ocular infection.

Corneal endothelial cells

The corneal endothelial cell density (ECD), average area, standard deviation, coefficient of variation, and hexagonality measurements were performed by specular microscopy (SP-3000P; TOPCON, Japan),and ECD was counted to evaluate the corneal endothelial damage before and after drug intervention.

Tissue preparation and histology

Animals were anesthetized and euthanized 6 days after intracameral injection. Two blank control eyes, 2 negative control eyes (5–10 μg of NC-siRNA complexed with 3 μL of LIPO), and 2 experimental eyes

(5–10 μg of IκBα-siRNA complexed with 3 μL of LIPO) were immediately enucleated, washed in cold saline, fixed in FAS eye fixative (Wuhan Servicebio, Wuhan, China) for at least 24 h, embedded in paraffin, and cut into 4-μm sections. Some sections were stained with hematoxylin and eosin (H&E) and modified Masson trichrome stain (Bioss, Beijing, China), and others were used for later IF. The H&E− and Masson-stained slides were examined to detect pathological changes in the cornea, TM and retina using a light microscope (Axio Planz imaging; Zeiss, Germany). Another 1 negative control eye and 1 experimental eye were immediately enucleated and washed in cold saline. Then, the MTM and MCM were dissected quickly on ice and preserved at −80°C for follow-up qPCR.

Histological immunofluorescence

The paraffin sections from 2 negative control eyes and 2 experimental eyes were sequentially dewaxed and hydrated, and antigen was retrieved with 10 mM sodium citrate. The sections were then incubated in 3% hydrogen peroxide for 20 minutes and permeabilized in 0.3% Triton X-100 for 20 minutes. Each section was blocked with 10% normal goat serum for 1 hour at RT and then incubated with primary antibody overnight at 4 °C. After three rinses in TBST, the slices were incubated with the corresponding secondary antibodies at RT for 40 minutes in the dark. After three washes, mounting medium with DAPI (Abcam, Britain) and coverslips were applied, and images were taken under a laser confocal microscope. The experiment was repeated 3 times for each eye for subsequent statistical analysis.

QUANTIFICATION AND STATISTICAL ANALYSIS

The statistical results of all experimental data *in vitro* were from independent three repeated experiments. Statistical analysis was performed using Prism 8.0 (GraphPad Software, San Diego, CA, USA). Data were expressed as mean ± standard deviation (SD). Differences between two groups were compared using Student's *t* test. Multiple comparisons were calculated using one-way ANOVA. Data were considered statistically significant at $p < 0.05$ (*$p < 0.05$, **$p < 0.01$, ***$p < 0.001$).